13C.3 MAPPING GLOBAL VEGETATION PHENOLOGY USING 1 KM MODIS DATA

Xiaoyang Zhang*, Mark A. Friedl, Crystal B. Schaaf,
Alan H. Strahler, John C. F. Hodges, and Feng Gao
Boston University, Boston, Massachusetts

ABSTRACT. Remote sensing can play an important role in phenological studies by monitoring the activity of vegetation communities at large spatial scales. Using data from the Moderate Resolution Imaging Spectro-radiometer (MODIS) acquired in 2001, we calculate the number of modes and key phenological transition dates, and examine spatial variation in phenological patterns on a global basis. To do this, a sigmoidal vegetation growth model is used to separately fit the increasing and decreasing sections of an annual trajectory of MODIS enhanced vegetation index (EVI) data. Extreme values in the curvature change rate are derived from the fitted growth model to automatically determine both phenological transition dates and cycle modality.

1. INTRODUCTION

Determination of global intra-annual vegetation phenology is important to models of terrestrial ecosystems, carbon exchange budgeting, and global climate change (Myneni et al. 1997; Schwartz 1999; White et al. 1997). Time series of normalized difference vegetation index (NDVI) data from the Advanced Very High Resolution Radiometer (AVHRR) have been widely applied for monitoring the dynamics of vegetation. However, these data have proven to be limited since AVHRR NDVI data saturate at relatively low values of leaf area index, possess poor geometric registration, are not atmospherically corrected, possess cloud contamination effects, and are affected by bi-directional effects and high-view angle biases (e.g. Goward et al. 1991; Reed et al. 1994). Using time series of AVHRR NDVI data, a number of different methods have been developed for phenological analysis (Table 1). These methods work well at local and regional scales, or for specific vegetation types. However, these methods are difficult to implement globally since they involve empirical constants that are applied globally, and therefore generally do not account for ecosystem specific characteristics of vegetation growth.

Globally, multiple growth cycles may exist in agricultural, where double- or triple-cropping is common. Further, in semi-arid regions vegetation growth follows the annual cycle of precipitation, which can be characterized by multiple rainy seasons, although one cycle is often dominant. In a typical cycle, four successive phases of vegetation phenology (depending on both climate and ecosystem type) can be remotely sensed: greenup, maturity, senescence, and dormancy. These periods can be defined by the transition date of onset of vegetation growth (Gd), the subsequent date of maturity onset (Md) with plant green leaf area reaching maximum, the date of onset of senescence (Sd), and the date of onset of full dormancy (Dd). The goal of this study is to identify the number of growth cycles and key phenological transition dates, and to examine the spatial variation of phenological patterns at a global scale. To do this, an annual time series of Moderate Resolution Imaging Spectroradiometer (MODIS) data are used. The temporal trajectory of vegetation index is bisected into increasing and decreasing sections using a moving window technique. A sigmoidal growth model is then used to fit each section and to identify corresponding vegetation phenological variables. Finally, geographic patterns of the global phenological variation are related to spatial patterns in climate forcing.

Table 1. Methods currently used for phenology analysis in remote sensing

Method	Reference
NDVI threshold	Lloyd 1990
Backward-looking moving averages	Reed et al. 1994
Largest NDVI increase	Kaduk and Heimann 1996
Best fit line in a 70 day period	Duchemin et al. 1999
Normalized NDVI ratio >0.5 for greatest increase (onset) and decrease (offset)	White et al. 1997
Lowest value calculated from the derivative within five weeks and empirical coefficients	Moulin et al. 1997

2. MATERIALS AND METHODS

2.1 *MODIS Data*

The MODIS instrument possesses seven spectral bands that are specifically designed for land applications with spatial resolutions ranging from 250 m to 1 km. These data are atmospherically corrected, cloud masked, and geometrically rectified. Using daily multi-angle surface reflectances collected over 16-day periods, one nadir BRDF (bi-directional reflectance distribution function) adjusted reflectance (NBAR) is generated for each MODIS land band at 1-km spatial resolution (Schaaf et al. 2002). The data set used for this analysis includes one year of NBAR data for the period from 1 January to 31 December 2001. Unfortunately, however, NBAR data were not acquired between 10 June and 11 July 2001 (two 16-day periods), due to instrument problems.

Because the enhanced vegetation index (EVI) has several advantages over NDVI (such as reduced sensitivity to soil and atmospheric effects), EVI were calculated for each 16-day NBAR based on the method

* *Corresponding author address*: Xiaoyang, Zhang, Boston Uni., Dept. of Geography/Center for Remote Sensing, 725 Commonwealth Avenue, Boston, MA 02215 USA; email: zhang@crsa.bu.edu

developed by Huete et al. (2000).

Since EVI values for snow-covered surfaces differs significantly from those of soils and vegetation, information on snow cover is required. When more than half of the days in any given 16-day period are detected as snow covered, a snow flag is stored in the Quality Assurance (QA) field of the MODIS NBAR product. This provides a mechanism to flag snow covered areas.

Global climatic data are important to this study, since they are essential for illustrating the response of phenological variables to climate change. To this end, MODIS daytime Land Surface Temperature (LST) data with the same temporal and spatial resolution as MODIS NBAR data were compiled for this study. In addition, monthly precipitation data with a spatial resolution of 0.5 degrees were acquired from the Global Ecosystems Database (GED, Kineman and Ohrenschall 1992). These precipitation data were interpolated from a time series of spatially independent station records.

2.2 *Processing of Annual EVI Time Series*

Processing of temporal NBAR EVI data was carried out in the following sequence: (1) detection of normal background EVI, (2) identification of decreasing and increasing sections, (3) curve fitting by means of a sigmoidal vegetation growth model, (4) calculation of phenological transition dates.

(1) *Detection of the normal background EVI*. For phenological analysis, we distinguish between changeable vegetation and background EVI. The background EVI is defined as the minimum and stable value for a pixel without flood or snow effects within a year. This means that the background EVI may differ in each pixel, depending on the nature of the surface (e.g., bare soil versus dormant vegetation). Snow is the main factor causing irregular EVI variation since it covers 43-47x10^6 km^2 between December and February in the northern Hemisphere (Gutzler and Rosen 1992). The presence of snow usually causes a dramatic drop in EVI value though the values are sometimes slightly higher than the background EVI when the snow reflectance in blue band is very high. When a (winter) snow period is identified based on the NBAR QA information, the EVI value is substituted with the most recent snow-free values.

(2) *Identification of decreasing and increasing EVI*. Prior to fitting a curve, it is necessary to identify periods of sustained EVI increase and decrease. To do this, a linear regression is applied within successive periods composed of five 16-day EVI values along an annual time series. Transitions from increasing to decreasing EVI trends are identified by a change from positive to negative slope within any given window, and vice versa. Slight decreases or increases of EVI may be caused by localized events such as drought or flooding instead of vegetation-growth cycles. To exclude such irregular variation, two rules are applied: (i) local EVI differences within a section should be larger than 35% of the annual EVI difference; (ii) local maximum EVI should be larger than 70% of annual maximum EVI. By calculating the number of increasing and decreasing sections, an arbitrary number of growth cycles can be produced for a given annual time series.

(3) *Curve fitting*. Sigmoidal growth models have been demonstrated to be effective for depicting vegetation growth curves (e.g., for LAI and biomass) as a function of time (or cumulative temperature) using various field measurements (e.g., Ratkowsky 1983). In particular, logistic models have been extensively used to fit vegetation growth data (Darroch and Baker 1990). Because satellite vegetation index (VI) data are strongly correlated with green leaf area index (LAI), green biomass, and percent green vegetation cover (e.g., Myneni et al. 1997), nonlinear regression can be used to fit the NBAR EVI of each temporal section to a logistic curve of vegetation growth:

$$EVI = \frac{c}{1+e^{a+bt}} + d \qquad (1)$$

where t represents time in Julian days, a and b are the parameters associated with the rate of change in EVI, c is the maximum EVI value for a given period of vegetation growth, and d represents the initial background value. The four curve parameters were estimated using a least-square method for each section of vegetation growth. The fit was assessed using the root mean square (RMS) error and regression coefficient (R^2) between original data and model estimates.

(4) *Identification of phenological transition dates*. Time series of EVI change from one approximately linear stage to another when vegetation transitions between phenological phases. Therefore, the curvature-change rate (CCR; i.e., the derivative of curvature) derived from the logistic model can be used to identify phenological transition dates.

Specifically, transition dates correspond to the times at which the rate of change in curvature in the EVI data exhibits local minima or maximums. During the growth period, when vegetation transitions from a dormant state to maximum leaf area, three extreme points in a section of EVI curve can be inferred from the CCR, which are associated with specific ecological activity (Fig.1). Two maximum values of CCR are associated with the onset of leaf growth and the onset of maximum leaf area. Minimum CCR values correspond to the time of most rapid vegetation growth. Transition dates indicating the onset of senescence and dormancy can be estimated in a similar fashion. Due to the diversity of global data, the EVI behavior in a few pixels may be very irregular, where the extreme points on the CCR go beyond a reasonable range for any given dates. In such cases, the dates corresponding to 90% of the minimal and maximal EVI, which are calculated from the fitted models for the corresponding section, are taken as the phenological transition dates.

2.3 *Spatial Covariation in Phenology and Climate*

LST maps and the resultant phenological maps (1 km) were re-projected to a common geographic projection with one-minute resolution. Zonal averages across one-minute latitude intervals were then computed. The mean

annual temperature (MAT) averaged from 16-day LSTs within one year was also calculated. The monthly precipitation was averaged for each 0.5 degree latitude zone, and the start and end dates (month) for the rainfall season were calculated based on thresholds of 20, 40 and 60 mm/month respectively.

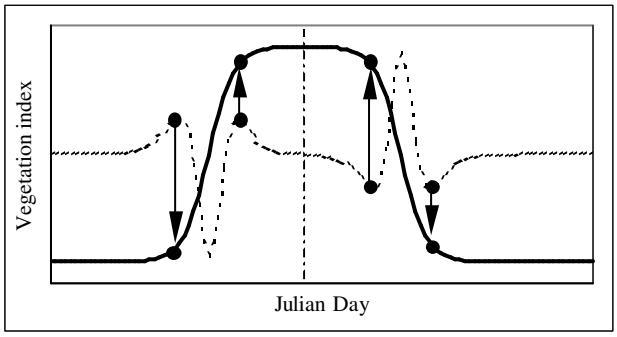

Fig.1. A schematic showing how transition dates are calculated using minimum and maximum values in the rate of change in curvature. The solid line is an idealized time series of a vegetation index, and the dashed line is the curvature change rate from the VI data. The circles indicate transition dates.

3. RESULTS

Using the methods described above, the four phenological transition dates for up to two annual cycles were produced globally. The estimated transition dates were highly variable geographically, suggesting that complex interactions among environmental effects such as land cover, temperature, precipitation and human activities contribute to phenological variation at this scale.

3.1 EVI Curves for Typical Land Cover Types

Representative samples of EVI curves for several IGBP (International Geosphere-Biosphere Programme) land cover types in the northern United States were selected to demonstrate the curve fitting procedure and calculation of phenological transition dates. These types include evergreen needleleaf forests (IGBP1), deciduous broadleaf forests (IGBP4), mixed forests (IGBP5), grasslands (IGBP10), cropland (IGBP12), and cropland/natural vegetation mosaics (IGBP14). While the biological interpretation of the model parameters is complex, *a* is positive and *b* is negative during EVI increase, and vice versa during EVI decrease (Table 2). For all cover types the RMS error was smaller than 0.04, and R^2 is larger than 0.95. The estimated phenological transition dates (Gd, Md, Sd, and Dd) for each curve are visually realistic (Fig. 2). These results indicate that the logistic model both provides a good fit to the temporal EVI pattern and is also able to realistically estimate the phenological transition dates.

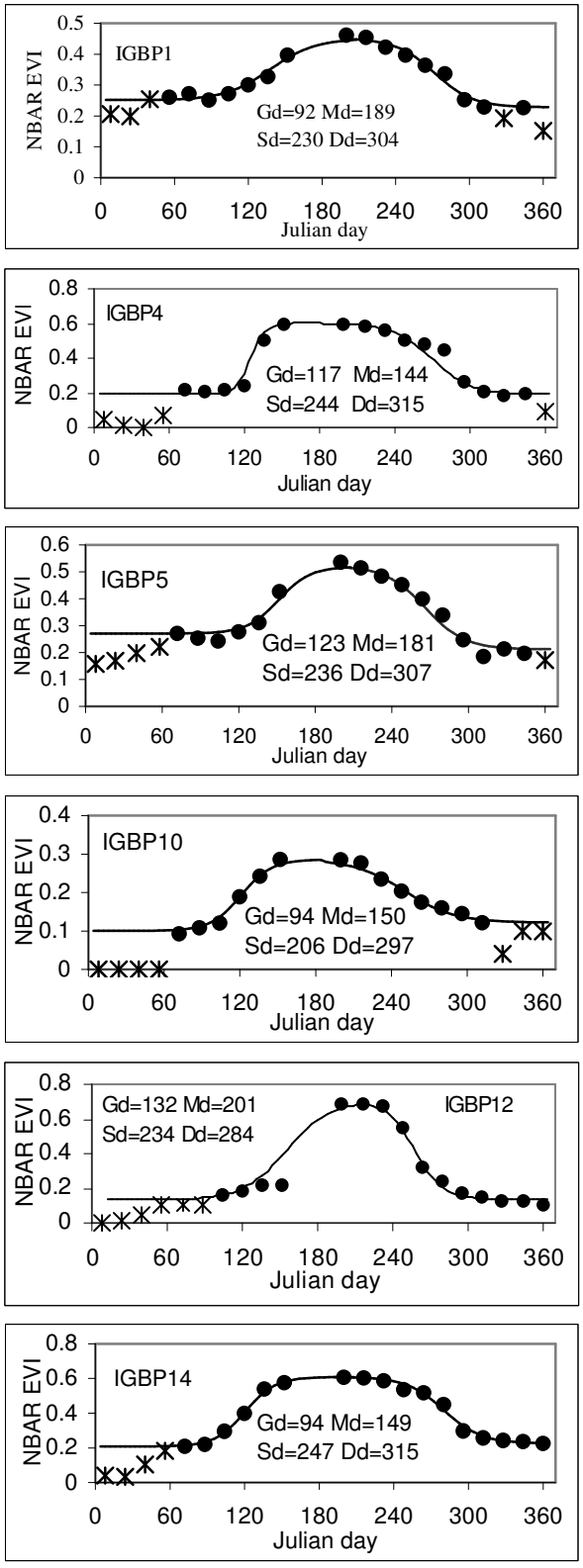

Fig. 2. Logistic curves (solid lines) fitted to the NBAR EVI values (dots) for several IGBP land cover types in the northern USA. The stars indicate EVI values during snow periods when negative values are set to zero.

Table 2. Estimated coefficients and goodness of fit for curves in figure 2.

	Increase section				Decrease section				Fitness	
Land cover type	a	b	c	d	a	b	c	d	RMS	r^2
IGBP1	5.61	-0.074	0.15	0.29	-4.99	0.062	0.18	0.27	0.013	0.97
IGBP4	28.7	-0.170	0.41	0.19	-8.09	0.064	0.44	0.19	0.036	0.95
IGBP5	6.16	-0.078	0.23	0.28	-5.70	0.073	0.23	0.28	0.022	0.97
IGBP10	8.08	-0.083	0.19	0.10	-4.14	0.050	0.16	0.12	0.009	0.99
IGBP12	7.55	-0.058	0.57	0.13	-5.30	0.091	0.57	0.14	0.033	0.98
IGBP14	6.65	-0.083	0.40	0.21	-6.43	0.067	0.38	0.23	0.016	0.99

Multiple growth and senescence cycles are most prevalent in the croplands of eastern China and in semiarid shrublands, grasslands in southern South America and Africa. Double crops in eastern China are used here to illustrate the estimation of multiple phenologic modes using piecewise logistic models (Fig. 3). The first crop cycle starts in February, with transition dates of Julian day 47,81, 124 and 145, respectively. The second cycle begins in early July with corresponding transition dates of 186, 209, 245 and 281 although the estimates of this second greenup onset may not be very accurate because of the data missing in June. The overall RMS error for the fitness is 0.022 and the R^2 is 0.98 between the original EVI data and the fitted models.

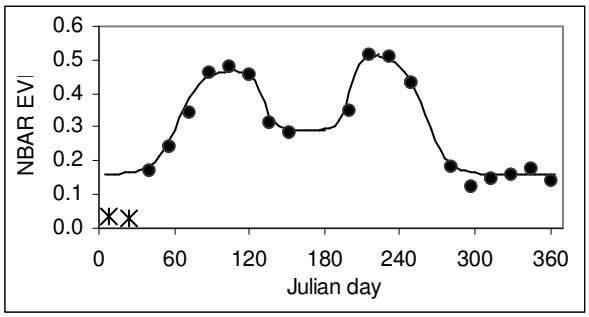

Fig. 3. Logistic curve (solid line) fitting to the annual EVI values (dots) for a cropland pixel in eastern China. The stars indicate the EVI values during snow period.

3.2 Temperature Driven Changes in Phenology in Northern High Latitudes

Changes in phenologic patterns are apparent north of 38°N, and are associated with seasonal temperature variations. As expected, greenup onset occurs earlier (in March) in the southern USA (south of 40°N), in April in the northern USA, and in June in northern Canada (Fig. 4). Dormancy onset spreads southward starting in late September in northern areas, reaching the southern USA in early November. This pattern changes in the Great Plains because of agriculture, where greenup occurs more than one month later than surrounding natural vegetation. Statistical analysis reveals that a 1.0° increase in mean annual temperature results in a 2.7 day advance in greenup and a 2.3 day delay in dormancy in North America (Fig. 4). A similar pattern is observed in Eurasia.

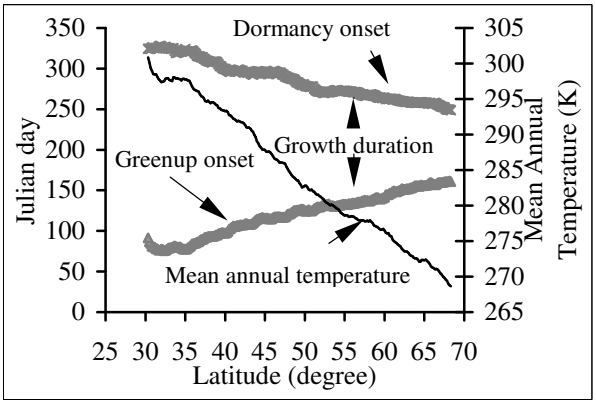

Fig. 4. Variation in average phenological dates and temperature along one-minute latitude intervals in North America.

3.3 Vegetation Phenology and Seasonal Rainfall

Vegetation phenology strongly coincides with rainfall seasons in many areas. In Mediterranean regions and the southwest USA, the main growth of vegetation occurs in winter, spring, and the summer monsoon season. In these areas, vegetation is greatly stressed during summer because of limited soil moisture. Outside of the equatorial regime, grass, shrub and savanna are the dominant vegetation types in Africa and southern South America, where water availability restricts the growth of green vegetation.

One of the most notable regions in which precipitation regimes influence vegetation activity is the Sahelian region in Africa, where phenological patterns depend strongly on precipitation and latitude. In this region, greenup typically starts in late July around 16°N and gradually advances southward to around 4.5°N in early March. This trend closely follows the rainfall season when monthly precipitation is larger than 20-40 mm (Fig. 5a). After about four to seven months, dormancy begins. The spatial trend in EVI data for the period considered shows that dormancy starts early in early November just south of the Sahara desert, gradually shifts southward to about 9°N in early December, and then shifts to earlier dates southward. This pattern matches the latitudinal pattern when rainfall decreases to less than 20-40 mm/month, especially in the northern regions (Fig. 5b).

In contrast, vegetation greenup starts at the end of September south of tropical forest, shifts progressively later (to the end of October) in the region around 17°S, and occurs earlier again at a rate of 22 days per degree of latitude in the region between 23°S and 33°S. Changes in the onset of greenup seem to be strongly associated with a threshold of 20 mm of precipitation. Dormancy onset begins in July with a small oscillation in this area. The rainfall data reveal that plants do not start their dormant phases until the dry season with monthly rainfall less than 20 mm lasts about two months, while the spatial pattern of dormancy onset is still correlated to the start of dry season.

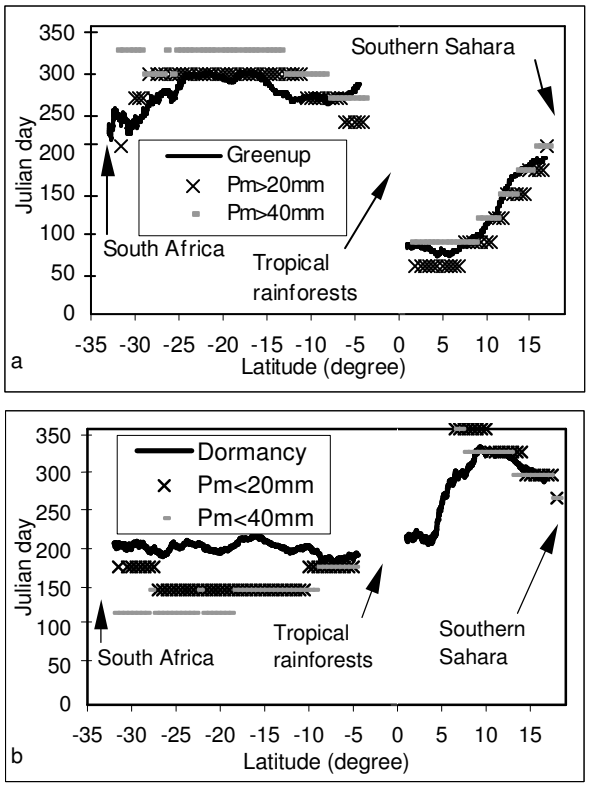

Fig. 5. Variation in average phenological dates with the starting and ending dates of rainfall season in Africa. Pm represents the monthly precipitation. a). Greenup onset, b). dormancy onset.

4. SUMMARY

The logistic model of vegetation growth provides a flexible means to monitor vegetation dynamics at global scales using remote sensing. The methodology presented in this work has several desirable properties. First, the behavior of the EVI data is described using a vegetation growth model, which is ecologically meaningful. Second, it treats each pixel individually without setting thresholds or empirical constants, so that the method is globally applicable. Finally, it is capable of identifying phenologic behavior characterized by multiple growth and senescence periods within a single year.

The results show that the MODIS-based estimates of phenological transition dates are geographically and ecologically consistent over the globe. In particular, the greenup wave gradually pushes northward and dormancy spreads southward above 38°N in the northern Hemisphere. These changes strongly coincide with temperature trends. Water availability results in a spatially irregular distribution of phenology in semiarid areas. Trends of phenological transition dates in Africa reveal that vegetation greenup onset follows the starting month of the rainfall season while dormancy onset begins after the dry season has begun for more than one month.

Acknowledgments. This work was funded under NASA contract number NAS5-31369.

REFERENCES

Goward, S.N., B. Markham, D.G. Dye, W. Dulaney, and A.J. Yang, 1991: Normalized difference vegetation index measurements from the Advanced Very High Resolution Radiometer. *Remote Sens. Environ.*, ***35***, 257-277.

Huete, A., K. Didan, T. Miura, and E. Rodriguez, 2002: Overview of the radiometric and biophysical performance of the MODIS vegetation indices. Special Issue, *Remote Sens. Environ.*, in press.

Kaduk, J., and M. Heimann, 1996: A prognostic phenology model for global terrestrial carbon cycle models. *Climate Res.*, ***6***, 1-19.

Lloyd, D., 1990: A phenological classification of terrestrial vegetation cover using shortwave vegetation index imagery. *Int. J. Remote Sens.*, ***11***, 2269-2279.

Moulin, S., L. Kergoat, N. Viovy, and G. G. Dedieu, 1997. Global-scale assessment of vegetation phenology using NOAA/AVHRR satellite measurements. *J. Climate*, ***10***, 1154-1170.

Myneni, R.B., C.D. Keeling, C.J. Tucker, G. Asrar, and R.R. Nemani, 1997: Increased plant growth in the northern high latitudes from 1981-1991. *Nature*, ***386***, 698-702.

Ratkowsky, D.A., 1983: *Nonlinear Regression Modeling-A Unified Practical Approach* (pp61-91). Marcel Dekker, Inc., New York and Basel.

Reed, B.C., J.F. Brown, D. VanderZee, T.R. Loveland, J.W. Merchant, and D.O. Ohlen, 1994: Measuring phenological variablity from satellite imagery. *J. Veg. Sci.*, ***5***, 703-714.

Schaaf, C.B., F. Gao, A.H. Strahler, W. Lucht, X. Li, T. Tsang, N. Strugnell, X.Y. Zhang, Y. Jin, J.P. Muller, P. Lewis, M. Barnsley, et al., 2002: First Operational BRDF, Albedo and Nadir Reflectance Products from MODIS. Special Issue, *Remote Sens. Environ.*, in press.

Schwartz, M. D. 1999: Advancing to full bloom: planning phenological research for the 21st century. *Int. J. Biometeo.*, ***42***, 113-118.

White, M.A., P.E. Thornton, and S.W. Running, 1997: A continental phenology model for monitoring vegetation responses to interannual climatic variability. *Glob. Biogeoch. Cyc.*, ***11***, 217-234.

Darroch, B.A., and R.J., Baker., 1990: Grain filling in three spring wheat genotypes: Statistical analysis. *Crop Sci.* ***30***, 525-529.

Kineman J.J., and M.A. Ohrenschall, 1992: Global Ecosystems Database, Version 1.0 (on CD-ROM). NOAA, Boulder, Co.

Uattzler, D.S., and R.D. Rosen, 1992: Internal variability of wintertime snow cover across the northern-Hemisphere. *J. Climate*, ***5***(12), 1441-1447.

Duchemin, B., J. Goubier, and G. Courrier, 1999: Monitoring phenological key stages and cycle duration of temperate deciduous forest ecosystems with NOAA/AVHRR data. *Remote Sens. Environ.*, **67**, 68-82.